Development of polymeric/MXenes composites towards 3D printable electronics

Composites Part B 263 (2023) 110854

Contents lists available at ScienceDirect

Composites Part B

journal homepage: www.elsevier.com/locate/compositesb

Development of polymeric/MXenes composites towards 3D printable electronics

Alejandra Salas [a], Hanna Pazniak [b], Jesus Gonzalez-Julian [c], Stefano Bianco [a], Julia Amici [a], Thierry Ouisse [b], Ignazio Roppolo [a,d,*], Matteo Cocuzza [a]

[a] Department of Applied Science and Technology, Politecnico Di Torino, Corso Duca Degli Abruzzi 24, 10129, Turin, Italy
[b] The Materials and Physical Engineering Laboratory, Grenoble INP, CNRS, Université Grenoble Alpes, F-38000, Grenoble, France
[c] Institute of Mineral Engineering, RWTH Aachen University, 52074, Aachen, Germany
[d] Centre for Sustainable Future Technology @Polito, Italian Institute of Technology, Via Livorno 60, 10144, Turin, Italy

ARTICLE INFO

Handling Editor: Prof. Ole Thomsen

Keywords:
$Ti_3C_2T_Z$-MXene
Polymeric composite
Photopolymerization
3D-printing
DLP

ABSTRACT

3D printing is an emerging technology for many applications, including electronics. On the other hand, to gather the applications' requirements with the possibility to produce complex 3-dimensional structures, the development of novel 3D printable materials is necessary. In this context, herein it is reported the synthesis of 3D printable photocurable resins embedding $Ti_3C_2T_z$-MXenes, a class of 2D layered materials with outstanding electrical and electronic properties. Stable inks suitable for Digital Light Processing 3D printing technology have been successfully synthesized and employed to fabricate complex 3D composite structures with high printing fidelity. To enhance the electrical conductivity of the material, annealing treatments have been performed, followed by a complete characterization of the so obtained materials. The results show that objects with improved electrical conductivity have been successfully obtained, opening new perspectives in towards the development of complex 3 dimensional electronic.

1. Introduction

2-Dimensional materials based on transition metal carbides, carbonitrides and nitrides, known as MXenes, have recently attracted large research interest due to their properties, such as high electrical conductivity, volumetric capacitance, hydrophilicity, and high thermal endurance [1–6]. Starting from pioneering works of Y. Gogotsi and M.W. Barsoum, such characteristics envisage promising performances in different fields like energy storage [7], electromagnetic shielding [8], photodetectors [9], sensors [10] and electrocatalysis [11]. MXenes are obtained from layered precursors known as MAX phase. Those are carbides, nitrides and carbonitrides, where M is an earlier transition metal (e.g. Ti, V, Cr, Nb, Y, Mo and Ta), A is an element of the A-group (e.g. Al, Si and Ga) and X is C and/or N [12]. MXenes are then produced by selective chemical etching of the A-element, in fluorine (F) or halogen (Cl, Br, etc.)-based environments. This process induces in the MXenes the presence of surface functional groups inherited from the etchants. After which, the formula of MXenes is $M_{n+1}X_nT_z$, where T_z comes from the terminations given by the acid solution or melts, typically = O, –OH, –F, and -Cl [13,14].

These termination groups determine the physicochemical properties of MXenes, for instance allowing better interaction with polymeric matrices, enabling the fabrication of MXenes-based composites [15–17]. These materials can combine the properties of polymers, such as good mouldability and processing, with the outstanding properties of MXenes such as the electrical and thermal response [18]. The interest towards MXenes is reflected in the number of published research articles, around 800 articles just in 2022 (source Scopus). For example, Qin L. et al. used the electrochemical polymerization process to develop MXene/composite films [19] for micro-supercapacitors. Shamsabadi, A.A. et al. developed membranes for CO_2 separation by embedding 2D $Ti_3C_2T_x$ nanosheets in Pebax®-1657 copolymer [20].

Beyond conventional manufacturing processes, additive manufacturing (AM) techniques, also known as 3D printing, can be used to develop MXene-based architectures [21]. This combination allows overcoming conventional 2D application of MXenes, achieving complexity in designs, accuracy, and fabrication of 3D objects from computer-aided design (CAD) data, via layer-by-layer processes [22].

* Corresponding author. Department of Applied Science and Technology, Politecnico Di Torino, Corso Duca Degli Abruzzi 24, 10129, Turin, Italy.
E-mail address: ignazio.roppolo@polito.it (I. Roppolo).

https://doi.org/10.1016/j.compositesb.2023.110854
Received 24 February 2023; Received in revised form 30 May 2023; Accepted 13 June 2023
Available online 14 June 2023

AM technology has been used to print MXene-based micro--supercapacitors [23], electrodes [24] and others [25]. Furthermore, polymeric composites containing MXenes were also employed in 3D printing [26,27].

Among the different 3D printing technologies, Digital Light Processing (DLP) and Stereolithography (SLA) [28] are known to be particularly suitable for the development of functional materials [25,29,30]. Those are based on light-induced polymerization, where a controlled light exposure generates radicals which, in turn, start a polymerization reaction which induces fast solidification of liquid resins. While SLA is based on the solidification of the resin caused by a laser beam causing localized polymerization of a photocrosslinkable polymer, DLP uses a two-dimensional pixel pattern that exposes and solidifies a full layer all at once [30]. This leads to faster print processes with good resolution [29,31]. For what concerns this investigation, few works are present in the literature related to light-induced 3D printing for MXenes-based inks, due to some intrinsic limitations. In fact, it is necessary to maintain the uniform distribution of the particles in the photocurable formulation during the printing process, avoiding sedimentation or aggregation which can affect the final properties [32,33]. Meanwhile, increasing the content of the nanoparticles may interfere within the photopolymerization since they compete with the photoinitiator in absorbing the incident radiation [34] and increasing the viscosity [35]. So far in previous works, 3D MXene-based structures have been printed either in particular conditions [36], with limited resolution [34] or in simple squared patterns for electrodes [24]. In this context, to the best of our knowledge only Fu. J et al. have achieved SLA printing with MXenes for scaffolds [25] while studies with DLP are not reported.

In this work, we aimed to explore this field, developing MXene-based inks, suitable for 3D printing vat-photopolymerization. This will lead to the applications of MXenes even in the fabrication of real 3D-objects, not limiting to conventional 2D geometry. Hence, we embedded MXenes in the printable formulations, to obtain complex and precise 3D geometries. The MXene composition used in this study is $Ti_3C_2T_z$ prepared by chemical etching of Ti_3AlC_2 in hydrofluoric acid (HF). These were later delaminated and introduced into a monomer formulation of Bisphenol A dimethacrylate (BPA-dma) and Trimethylolpropane triacrylate (TMPTA), whose reactions kinetics was studied by photorheology. Chemical characterization of the material and the resolution analysis of the printed structures through 3D scanning were performed. The choice of these monomers was based on their compatibility with an annealing post-process, which was further exploited to increase the electric conductivity of the 3D structures.

2. Methodology

2.1. Materials

All chemicals were purchased from Sigma Aldrich. The following monomers were used: Bisphenol A dimethacrylate (BPA-dma, >98%), and Trimethylolpropane triacrylate (TMPTA, containing 600 ppm monomethyl ether hydroquinone as an inhibitor). The Phenylbis(2,4,6-trimethylbenzoyl) phosphine oxide (BAPO, >97%) was used as the photoinitiator and acetonitrile (ACN, >99.9%) was used as the solvent.

2.2. MAX phase precursor

Ti_3AlC_2 MAX phase powders were synthesized from their elemental constituents by solid-liquid state reaction. Titanium (d50 = 24.8 μm, 99.0% pure), aluminium (d50 = 9.1 μm, 99.5% pure) and graphite (d50 = 6.9 μm, 99.0% pure) powders (all from Alfa Aesar) were used as starting materials and mixed in a molar ratio 3.0:1.1:2.0, respectively. An extra 10 wt % of the aluminium was added to compensate for its loss during the synthesis process at high temperatures. The mixture was heated up to 1350 °C for 3 h under an argon atmosphere to avoid oxidation. The synthesized Ti_3AlC_2 sample was ground in an agate mortar and milled in a planetary milling at 200 rpm in ethanol with zirconia balls (5 mm diameter) for 2 h. The resultant Ti_3AlC_2 powder presented a unimodal particle size distribution (d10 = 3.6 μm, d50 = 6.2 μm and d90 = 10.1 μm).

2.3. MXenes synthesis

The Ti_3AlC_2 MAX phase was etched under 49% HF, where 2 g of the powder was added slowly into a Teflon beaker containing 10 ml of the stirring acid. The mixture was kept for 5 h at room temperature under continuous stirring. The obtained solution was then transferred into a 50 mL falcon and repeatedly diluted with deionized (DI) water, centrifuged at 3500 rpm for 5 min, until the supernatant reached a neutral pH. The intercalation of the multi-layered structures was performed by adding 2 mL of 40% TBAOH (Tetrabutylammonium hydroxide) to the etched product and left stirring for 24 h. The delaminated suspension was washed in ethanol several times to get rid of the residual TBAOH until the neutral pH was reached. The $Ti_3C_2T_z$ MXenes were collected onto a polyvinylidene fluoride (PVDF) membrane (0.22 μm pore size) by vacuum filtration and left overnight on a vacuum dryer. Before using, MXene powder was dispersed in DI water and additionally sonicated at 49 kHz for 50 min in an ice bath under nitrogen bubbling. Then MXenes were collected by centrifugation at 3500 rpm for 30 min, recovering the supernatant, which was further used to prepare the ink.

2.4. Ink preparation

The formulations were prepared by mixing the monomers (BPA-dma and TMPTA), the photoinitiator (BAPO), solvent (ACN), and by adding the MXenes, in the quantities reported in Table 1, followed by sonication for 5 min. The percentages refer to the relative amount of each component in the final formulation.

2.5. 3D printing

The 3D Printing of the nanocomposites was performed on an ASIGA UV-MAX DLP printer with LED light source emitting at 385 nm. During the printing, the layer thickness was fixed at 50 μm for the burn-in and 70 μm for the successive layers, with the light intensity at 37 mW cm^{-2}. The exposure time was 21 s for the BPA-dma: TMPTA composite, and for the other composites 25, 30 and 35 s increasing the time with the MXene concentration. Finally, a post-curing process was performed on the printed samples. They were first washed with acetone to remove residual formulation and then exposed under a UV lamp (from Robot Factory) for 2 min, with a light intensity of 12 mW cm^{-2}.

2.6. Thermal treatment

Two types of thermal treatment were tested to evaluate the annealing process, one under inert conditions and the other under reductive ones. The first one involved heating for 5 h at 900 °C at a heating rate of 3 °C/min under an argon atmosphere with >50 ml/min gas flow in a tubular furnace using pure Ti metal as the oxygen getter. The same protocol was used for the reductive environment, but under a 5%

Table 1
Formulations.

Formulation	BPA-dma [wt.%]	TMPTA [wt.%]	MXenes [wt.%]	ACN [wt.%]	BAPO [phr]
BPA-dma: TMPTA	17	33	0	50	1
MXenes 1%	17	33	1	49	1
MXenes 2%	17	32	2	49	1
MXene 5%	17	29	5	49	1

hydrogen and argon atmosphere.

2.7. Characterization

To investigate the kinetics of the photocurable formulations, photorheology was performed using an Anton PAAR Modular Compact Rheometer (Physica MCR 302) in parallel-plate mode, equipped with a UV-light source (Hamamatsu LC8 lamp 15 mW cm^{-2}) under the bottom plate. The measurements were performed under isothermal conditions (25 °C) with a constant shear angular frequency (10 rad s^{-1}). The photoreactivity was investigated by following the changes in the storage moduli (G') during UV-light irradiation. The light was switched on after 60 s to stabilise the system before the polymerization onset. Meanwhile, the viscosity curves were taken on the same equipment changing to a rheometer modulus with shear rates in the range 0.001–100000 s^{-1}.

The UV–visible spectra were recorded by a Synergy™ HTX Multi-Model Microplate Reader Instrument (Biotek, Winooski, VM, USA) set in spectrum mode between 330 and 500 nm with a scan step of 1 nm. The experiments were performed on solid films of 200 nm, using a 24-well plate. The Fourier-transform infrared spectroscopy (FTIR) spectra were collected using a Tensor 27 FTIR Spectrometer (Bruker) equipped with an ATR (Attenuated Total Reflectance) tool. The average signal collected was in the range of 4000–500 cm^{-1} with a resolution of 4 cm^{-1}. For each sample, a background measurement was run before the analysis was performed on the liquid formulation ($t = 0$) and the solid films ($t = t_\infty$). The conversion of the acrylate double bonds was calculated following the decreased area of specific peaks. Both method's results are reported in the SI.

The morphology of the prepared composites was investigated by a Zeiss Supra 40 FESEM, equipped with a GEMINI II column and EDS analyzer, where a probe current of 1200 pA and an accelerating voltage between 5.00 and 15.00 kV were used. On the other hand, the surface composition was analyzed by a PHI 5000 Versaprobe Scanning X-ray Photoelectron Spectrometer (monochromatic Al K-a X-ray source with 1486.6 eV energy). The sample size was 100 μm for the high-resolution shift, exploiting 23.5 eV for these peaks. To reduce the charging effect during measurements, all samples were analyzed with a combined electron Ar-ion gun neutralizer system. X-Ray Diffraction (XRD) was used (Panalytical X'Pert Pro X-ray diffractometer) in Bragg/Brentano configuration with Cu Ka as an X-ray source to examine the crystalline structures. Finally, the Thermal Gravimetric Analysis (TGA) was performed to determine the degradation temperature in an inert environment, using a Mettler Toledo TGA with STARe software and placing the samples in alumina crucibles (70 μL). The resistance was measured through a voltage linear sweep method from −10 V to 10 V with compliance of 0.021 A using a Keithley 4200A SCS Parameter Analyzer. The samples used were 3D-printed with dimensions 10 × 10 × 5 mm^3 and then tested on a two-probe arrangement system, where both probes rested in contact with the sample's surface applying a slight pressure to avoid piercing or breakage.

The mechanical properties were evaluated using a Tritec 2000 DMA (Triton Technology Ltd, London UK). The measurements were conducted at 26 °C, with a force ramp of 1 N/min and a target force of 5 N. 3 sample were tested for each specimen, 3D printed samples were 10 × 10 × 1 mm^3, while the annealed shrinked versions were of (5 × 5x0.2 mm^3). From the measurements, Elastic Moduli (E) were extrapolated.

2.8. 3D scanning

was performed to evaluate print resolution compared to the original CAD file using a 3D optical scanner (E3, 3Shape). The scanned data and the reference model were aligned before the statistical comparison, and the analysis is displayed as a color 3D heatmap displaying the geometric deviation. The same software was used to measure and compare samples before and after annealing, to determine the surface area exposed and the volume of the printed samples.

3. Results & discussion

3.1. Evaluation of the 3D printability

To investigate the 3D printability of MXene inks based on acrylate monomers, photopolymerization kinetics was initially evaluated, Fig. 1 (a–d) show the schematic representation of the process. $Ti_3C_2T_z$ MXenes have a broad light absorption in UV–Vis range which overlaps the BAPO photoinitiator absorption (band from 350 to 430 nm [37]), as inferable from the UV–visible spectra in Figs. SI–1. This may reflect in a decrease in the efficiency of the photopolymerization mechanism due to a competitive absorption of incident light [31]. This effect was investigated using photorheology, following the change of viscoelastic properties after irradiation. Fig. 1(e) shows the changes in G' modulus (elastic modulus) for the different tested formulations. The photorheology demonstrates that formulations with higher concentrations of $Ti_3C_2T_z$ showed a slight delay after the start of the photopolymerization (see inset in Fig. 1(e)). Nevertheless, they showed similar G' values at the end of the reaction and stability at this stage, confirming their suitability for 3D printing. The presence of MXenes in the BPA-dma: TMPTA resin slows the reactivity of the photopolymerization, which confirms their photo-blocker activity [34]; in 3D printing procedure usually this translates into longer layer exposure. The photo-blocker effect is like the UV-shielding effect already measured for CNTs [38–40]. The effect of MXene on photopolymerization can also be observed in the double bond conversion in the FTIR spectra (Figs. SI–2), with a consistent decrease at the higher filler concentrations.

In Fig. 1(f) viscosities of the different formulations are reported. As expected, all the formulations showed a shear-thinning behaviour and an increase in viscosity with the increasing amount of MXenes. In standard DLP 3D printing, usually viscosity below 50 Pa s is requested [36], thus formulations containing 5% of MXene can be critical in the next investigation step.

On the other hand, the presence of MXenes can also be beneficial for 3D printing, acting similarly to functional dyes. In transparent resins the control of light penetration can be problematic, causing uncontrolled polymerization and consequently poor resolution of printed structures [41]. In DLP 3D printing, a dye is often used for limiting light diffusion. So far, in the literature, organic functional dyes have been reported [42] to add properties likewise, but also inorganic materials were exploited such as silver nanoparticles [43], graphene oxide [41] and others. In this case, MXenes, can also play a role in this direction, since they give a blackish pigmentation, limiting also light penetration and allowing better control of the reaction.

Once stable formulations were developed (Fig. 2(a)) and their behaviour under irradiation was investigated, these were used to produce 3D printed structures like the one shown in Fig. 2(b) and Figs. SI–3. Each formulation required an optimization of the printing parameters, as reported in the method section. As expected after photorheology tests, longer layer irradiation times are necessary for the formulations containing the fillers. Fig. 2(b) demonstrates the good CAD fidelity of formulations with 2 wt %. MXenes (see also Figs. SI–3 for 5 wt%). Therefore, complex MXenes-based architectures can be printed showing a good resolution, and exemplary structures like lattice cube and honeycomb were reproduced. Such complex geometries can be then envisaged and designed for advanced electronical applications, nevertheless, to this perspective also electric and electronic performance must be evaluated.

Hosting polymeric matrix is an insulating material and the presence of 2 wt% MXenes decreases resistance from 1468.4 to 507.6 G Ω (see Table 2 later), however, those 3D printed structures are still not suitable for an electronic application. To obtain conductive structures should be thus necessary to increase considerably the content of MXenes as well as the conductivity of the hosting matrix. For this aim, Tetik. H et al. exploited direct inkjet printing and freeze casting [36], while Yang. W et al. [44] used extrusion-based 3D printing and freeze-drying to

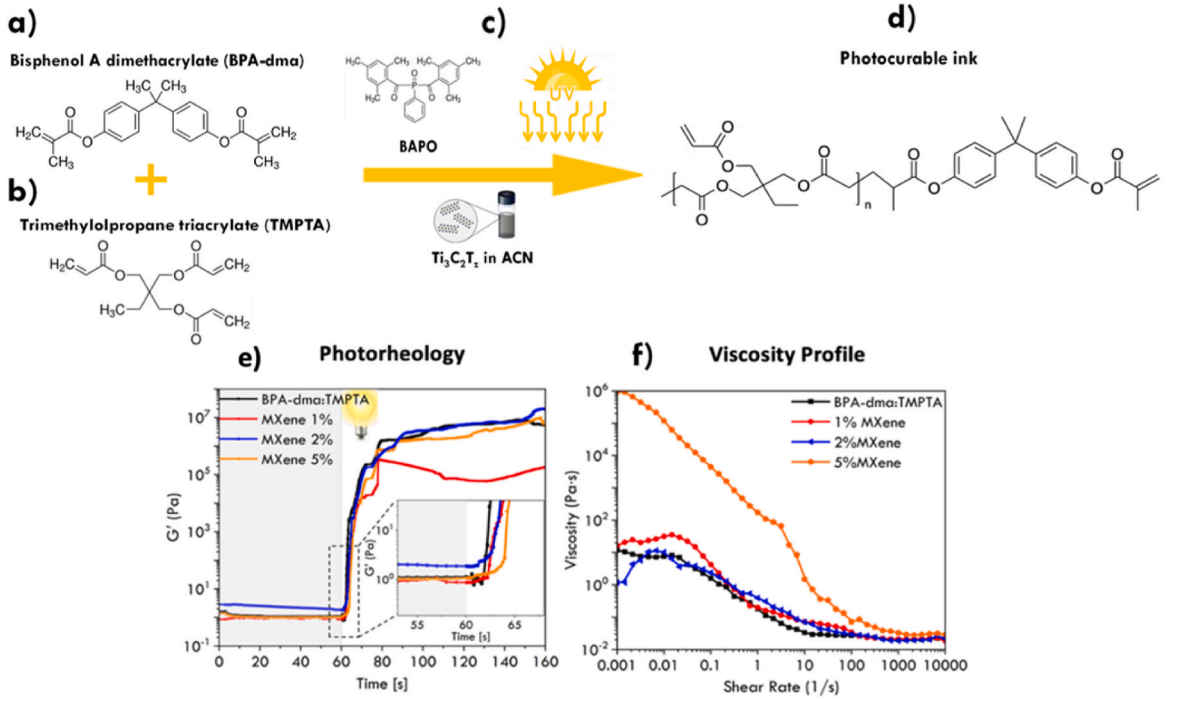

Fig. 1. Chemical formula of a) BPA-dma and b) TMPTA, c) BAPO chemical formula and the schematic representation of the preparation process, d) representation of the final polymer, e) photorheology and f) viscosity profile of the given formulations.

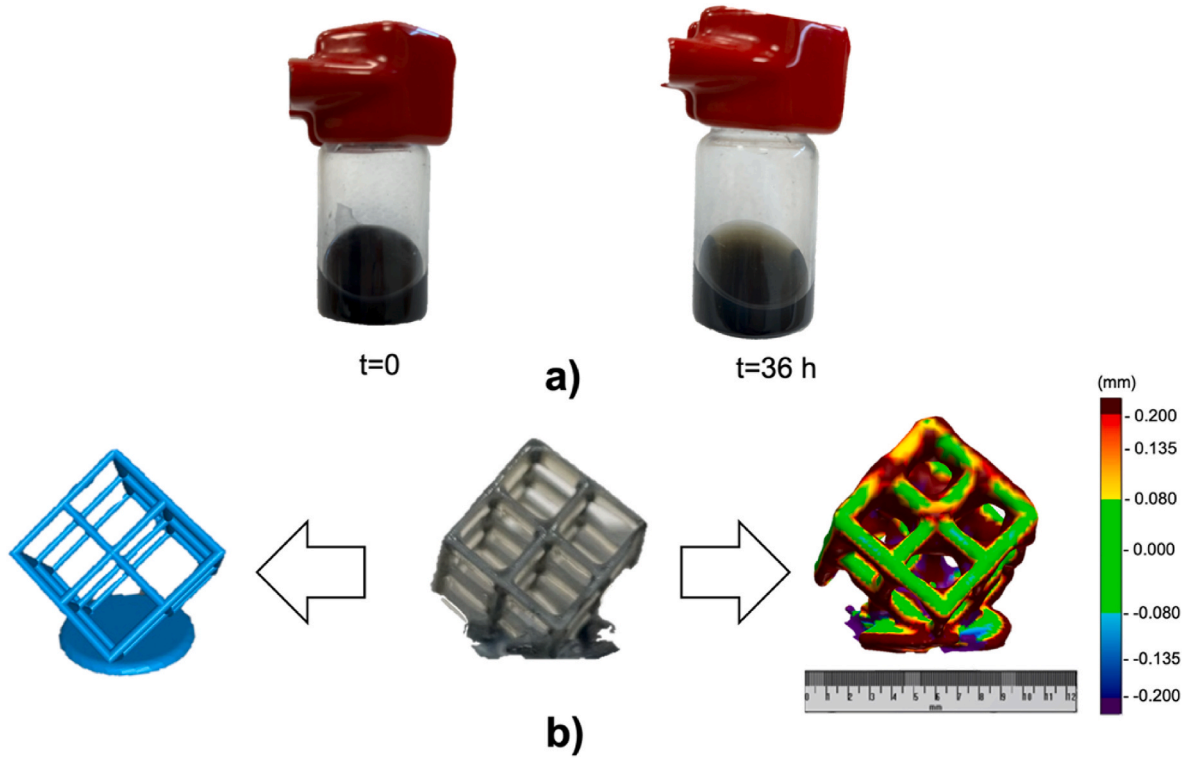

Fig. 2. a) Stability of the liquid formulation up to 36 h and b) figure from the CAD to the printed structure and its 3D scanning.

withhold MXenes architectures with good conductivity.

In the present case, a further increase in the content of MXenes will have the previously mentioned limitations in terms of printability. So, our strategy focuses first on 3D printing using an ink that includes monomers, like TMPTA and BPA-dma, with a low amount of oxygen for later, as a second step, inducing annealing. In fact, it is well-reported that carbonization of polymeric structures can lead to an increase in electrical conductivity [45,46]. Consequently, we followed this strategy with a twofold goal: (i) increase the conductivity of the matrix; (ii) increase the relative content of MXenes in the composites due to thermal degradation of some part of the polymeric structure. Accordingly, the MXenes content should increase in the final composites, with further

Table 2
Resistance measurements.

Sample	Resistance (GΩ)
Polymer Matrix (BPA-dma: TMPTA)	1468.4
Polymer Matrix (carb.)	261.8
MXene composite 5 wt%	507.6
MXene composite 5 wt% (carb.)	10.5

conductivity enhancement. The thermal treatments were performed either under an inert or reductive atmosphere, and those were compared in terms of materials characteristics and shrinkage of the structures.

3.2. Thermal treatment of 3D printed MXenes composites

TGA measurements (Fig. 3(a)) were initially performed in an inert atmosphere, to simulate the thermal process in the oven. As can be observed, the polymeric matrix undergoes thermal degradation with a consistent mass loss between 400 °C and 500 °C, while the mass of MXenes is slightly reduced from 50 °C to 400 °C, associated with the loss of water and some surface functional groups, and almost constant from 400 °C to 900 °C as seen on the black curve and on the respective composites. The same thermal behaviour of $Ti_3C_2T_z$ in an argon atmosphere was observed by M.Han et al. [47]. The presence of the MXenes seemed to slightly delay the degradation towards higher temperatures. Most importantly, a certain residue can be measured at the end of the process, which in the case of pure polymeric matrix was around 3 wt% of the initial mass and with MXenes is higher than 10 wt% This can be consistent with a barrier effect of MXenes towards volatilization of degradation by-products during the thermal process, which leads to carbonization. On the other hand, TGA measurements cannot provide information on the structural modifications of the materials, and to this aim XRD, XPS and FESEM experiments were performed.

The results of the XRD analysis of the polymeric matrix, the pure $Ti_3C_2T_z$ MXenes obtained from the Ti_3AlC_2 MAX phase by the Al removal and of the MXene/composites are shown in Fig. 3(b). Polymeric matrix (Fig. 3 (b), black curve) shows the expected amorphous behaviour.

Concerning pure MXenes, yellow and green curves in Fig. 3 (b) show the spectra after synthesis and after thermal treatment in an inert atmosphere at a temperature of 600 °C respectively. Typical (002), (004) and (006) peaks of MXenes are clearly detectable in both spectra, while the corresponding SEM image of delaminated flakes are reported in Fig. 4(a). Furthermore, traces of oxidation are present. According to Li. Z et al. [48], the first oxidation stage involves the oxidation of the MXenes surface layers, where the TiO_2 anatase form appears first, as evident in the yellow curve. Despite the inert atmosphere, thermal treatment at 600 °C causes an evolution of the Ti oxidation process towards the formation of titanium dioxide in rutile crystallographic form. These newly formed nanocrystals are attached to the outer sheets and limit the contact of unreacted sheets with O_2, which in turn slows further oxidation and hinders the release of CO_2 produced by the titanium carbide degradation.

Fig. 3 (b) also shows the XRD spectra of composite materials at different concentrations (2 wt% MXene, blue curve, and 5 wt% MXene, orange curve). The fillers are clearly embedded into polymer matrix, as confirmed by the characteristic (002) and (004) peaks related to the lamellar structure of the MXenes. Fig. 3 (c) shows a schematic representation of the interaction between the polymer and the MXene in the composite, similarly to other composites with layered fillers. In this case, the material shows an increase in the interplanar distance, witnessed by the shift of the (002) peak towards smaller angles. This phenomenon is compatible with the typical behaviour of lamellar materials reported in the literature [49,50] and seems accentuated by the thermal treatment. In literature, it is also reported that when MXenes are exposed to temperatures up to 900 °C in inert atmosphere, moieties including –F, –OH groups are eliminated without affecting the layered structure, and maintaining the conductivity [51]. However, when embedded in a polymeric matrix, despite the inert atmosphere, the degradation of the polymeric matrix induces the generation of oxygen and hydroxyl radicals, which in turn can lead to MXenes oxidation as evidenced from the XRD patterns (Fig. 3 (b), light blue curve).

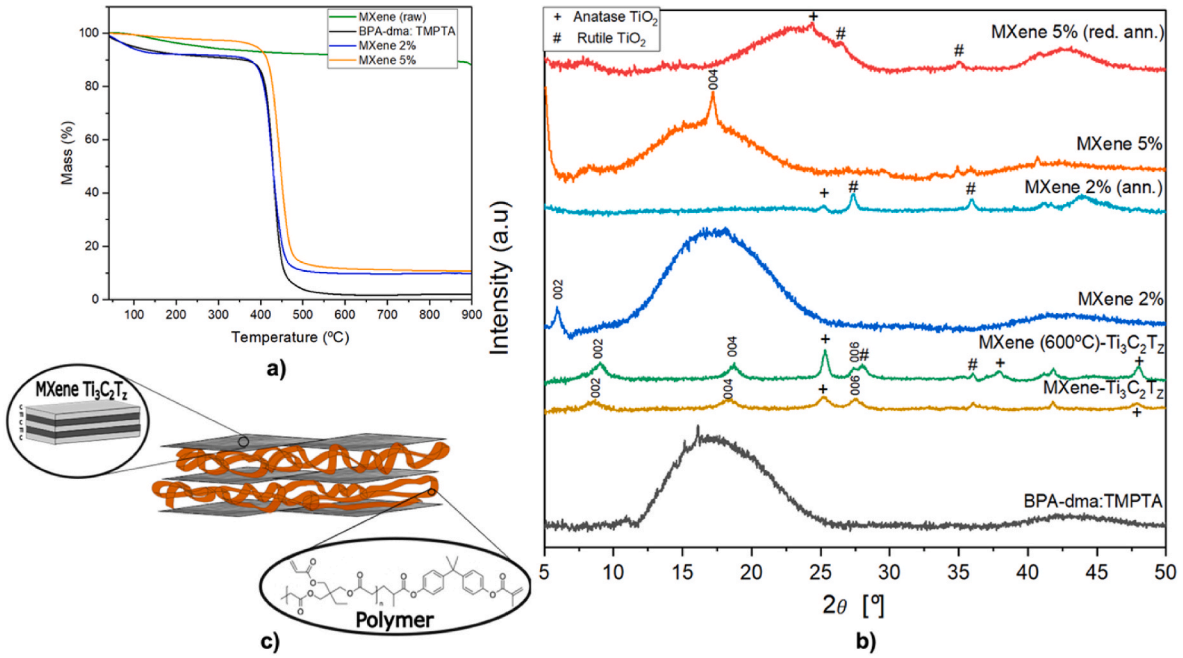

Fig. 3. (a) TGA in N_2 of the pristine MXenes sample (green), the composite BPA-dma:TMPTA (black), composite at 2 wt% (blue) and 5 wt% MXenes (orange) content. (b). XRD patterns of the BPA-dma:TMPTA (black), MXenes sample before annealing (yellow), after annealing (green), MXenes/composite at 2 wt% (blue), annealed MXene/composite 2 wt% (light blue), MXene/composite 5 wt% (orange) before annealing and after reductive annealing (red). (JCPDS cards: TiO2 anatase: 89–4921; TiO2 rutile: 89–4920) (c) Schematic representation of the interaction between polymeric matrix & $Ti_3C_2T_z$-MXene. (For interpretation of the references to colour in this figure legend, the reader is referred to the Web version of this article.)

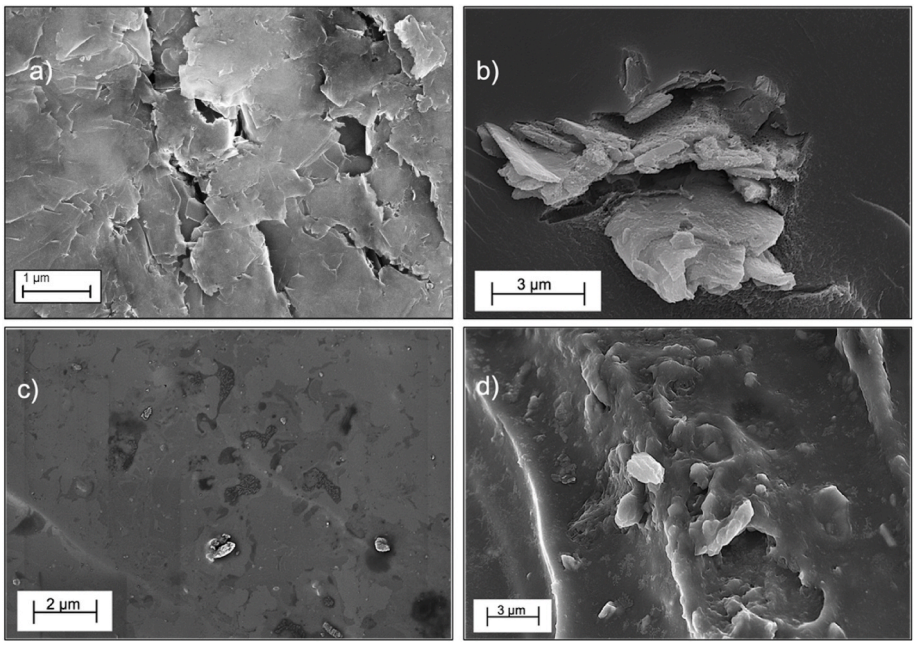

Fig. 4. FESEM images of: a) pure MXenes ($Ti_3C_2T_z$) delaminated sample; b) 5 wt% MXenes/composite before annealing; c) 5 wt% MXenes/composite annealed in a reductive environment; d) 5 wt% MXenes/composite annealed in an inert environment.

Moreover, high-temperature annealing treatments at 900 °C of the composite material in reducing environment have been carried out and the spectral characteristic are reported in Fig. 3 (b) (red curve). Also in this case, the characteristic peaks of the MXenes are no longer detectable, showing that the long-range order of the crystalline structure is lost during the treatment.

Fig. 4(a) shows the morphology of $Ti_3C_2T_z$ MXenes after delamination. A stacked structure of several translucent sheets of irregular shape is clearly observed when deposited on Si/SiO_2 substrate by drop-casting. When 5 wt% of MXenes are embedded in the composite, they are uniformly distributed in the matrix. However, there are some areas where MXenes agglomeration can be seen, as shown in the cross-section of the 3D-printed polymeric composite (Fig. 4(b)). Fig. 4(c) and (d) show the structure of MXenes/composite after annealing in a reducing and inert atmosphere respectively. The surface of the composites after annealing in both atmospheres looks identical and is quite homogeneous. MXenes sheets are not clearly visible on their surface.

XPS was also used to better characterize the composites. High Resolution (HR) Ti2p and C1s spectra are collected and compared in Fig. 5: concerning the HR Ti2p spectra, in the pure MXenes sample two main components are observed. The highest belongs to the Ti–C bond (constituted by a doublet at 455.7 eV and at around 462 eV), while the second and lower peak belongs to the TiO_2 at 460 eV. This second peak represents the different possible forms of Ti oxycarbides present on the surface given by the sample oxidation [52–54]. This can be related to spontaneous surface oxidation of $Ti_3C_2T_Z$ MXenes under environmental conditions, confirming XRD observations.

Differently, the printed composite shows a very low Ti–C signal with great dispersion at 455.6 eV, due to the low concentration of reduced Ti at the surface and the presence of TiO_2, evidenced by the 459.3 eV peak. This may suggest that MXenes are mainly embedded and not present on the composite surface. Meanwhile, the Ti bonds can be easily detected on the composite's annealed version, since most of the organic phase was thermally degraded, giving less dispersion and sharper peaks. On the other hand, the presence Ti–O peak, also observed from XRD, indicates a certain degree of oxidation of MXenes on the composites surface and after annealing, higher than in pure MXenes phase (Fig. 5(c)).

Regarding C1s spectra, on the pure MXenes sample (Fig. 5(a)) the Ti–C at 281.9 eV is the most relevant component, reflecting the (Ti_3C_2) bonds. Other components are also present at 285 eV, 286.8 eV and 289.5 eV, which were attributed to C–C, C–O and C═O bonds respectively [53–55]. In contrast, in the composite samples (Fig. 5(b)) the Ti–C was not detected, while peaks related to C–C, C–O and C═O were evidenced. The presence of those peaks is consistent with the observation of the polymeric matrix, supporting the description above mentioned on the low surface exposure of MXenes in this sample. In the annealed sample, the Ti–C peak is again observed, in good agreement with the other XPS measurements.

At last, mechanical properties of the MXenes/composite samples were tested and values of E (Elastic Modulus) are reported in Table SI1 (Supporting Information File). As expected, the presence of MXenes increases the Elastic Modulus of the composite (from 80 MPa to 300 MPa with 5% of MXenes), while it has a lower effect after thermal treatment, with the mechanical behavior that is mostly determined by carbonization process. In fact, the E value after thermal annealing for the neat polymeric matrix is 2 GPa, and 2.1 GPa in the presence of MXenes. These values, similar to polymers such as polycarbonate or polypropylene, may suggest the use of annealed 3D printed part also for not-demanding structural applications beyond the functional one.

3.3. Shrinkage of 3D printed structures

As expected for a thermal process, after annealing the 3D printed structure an evident shrinkage in the components was observed. This was measured by comparing the volume of the structures before and after the thermal treatment using 3D scanner. Fig. 6 depicts these shrinkage percentages in various 3D printed structures with and without MXenes. Shrinkage varies depending on the 3D structure, but for structures with MXenes it is about 75%. In this regard, these measurements suggest that the CAD design, and thus the printing, must be adjusted according to the volume of the final required device.

3.4. Resistance

The I–V measurements performed on the printed samples are shown in Fig. 7. As evident, the MXenes-containing composite after the reducing carbonization treatment is characterized by larger conductivity with respect to the other samples, which display similar low current

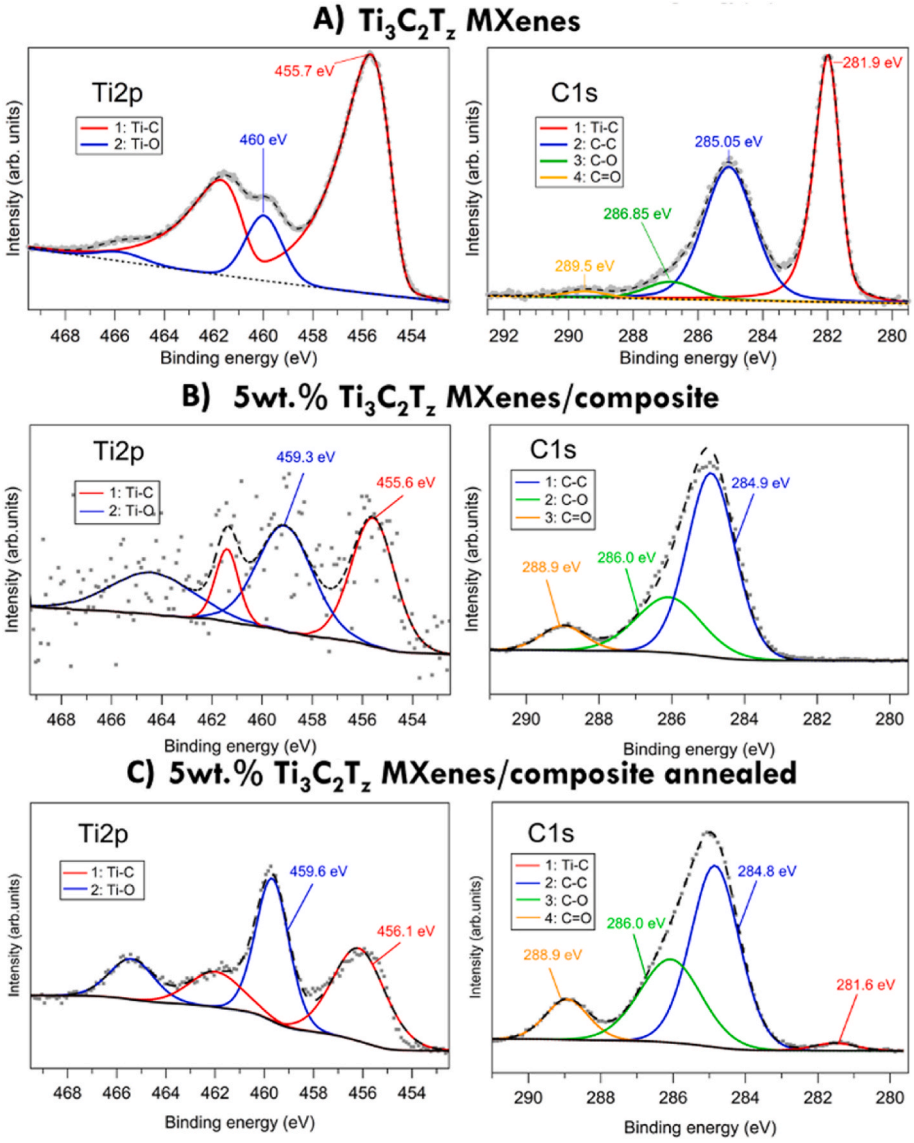

Fig. 5. XPS High-resolution spectra A) Pure MXenes sample, B) 5 wt%MXenes/composite and C) the annealed 5 wt%MXenes/composite. Each bond is represented in a specific colour line shown on the legends. (For interpretation of the references to colour in this figure legend, the reader is referred to the Web version of this article.)

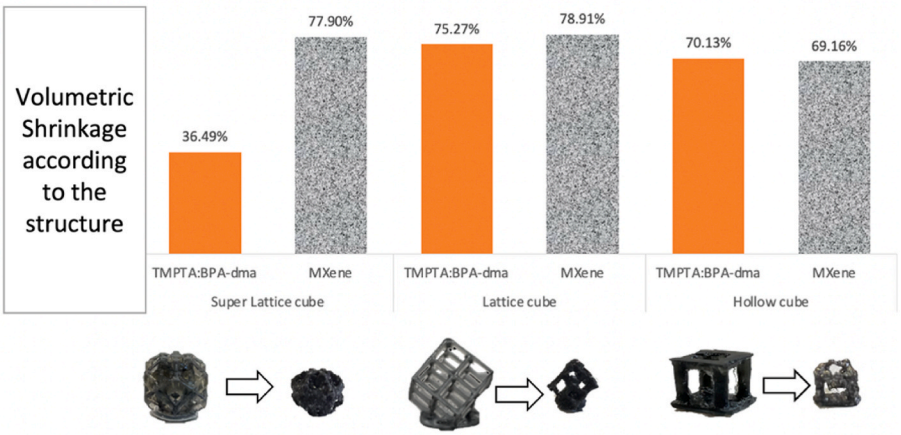

Fig. 6. Bar chart representation of the volumetric shrinkage of the structures with and without MXenes. On the bottom, the different printed nanocomposite structures are reported before and after the carbonization.

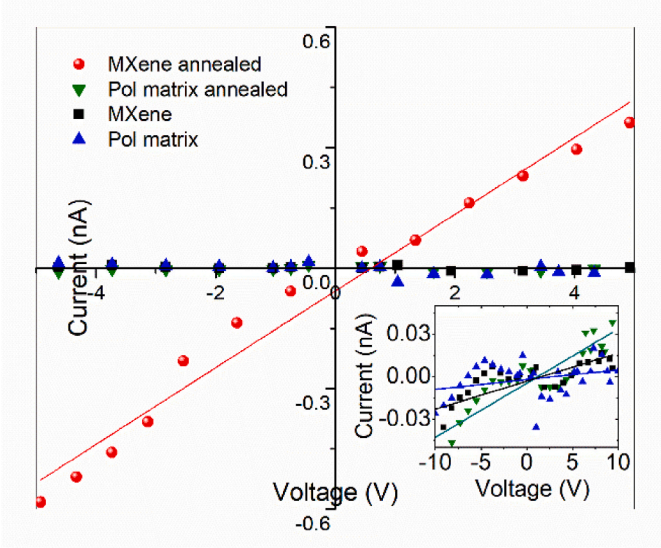

Fig. 7. I–V Measurements of the different samples.

values.

Moreover, it is important to highlight that the carbonization treatment is beneficial also to increase the conductivity of the bare polymeric matrix, as shown in the inset of Fig. 7.

The obtained I–V curves were fitted with straight lines to calculate their slope, and consequently, to evaluate the resistances of the different samples, which otherwise, would have been difficult to obtain because of the very noisy values due to the low conductivity of the samples by themselves. The obtained resistance values are reported in Table 2, demonstrating that the addition of the MXenes to the polymeric matrix has effectively increased its conductivity, which also became one order of magnitude larger after the thermal treatment.

4. Conclusions

In this work, the fabrication of printable MXenes nanocomposite polymers using DLP 3D printing is reported based on photocurable acrylate resins and containing $Ti_3C_2T_Z$ as a nanofiller. During the printing, higher light intensity and longer slicing time were needed due to the photo blocker activity of the MXenes, but the structures were achieved with high fidelity. However, nanocomposites did not show significant improvement in electrical properties compared to the neat polymeric matrix, thus carbonization process was performed on 3D-printed structures. This increases the relative amount of MXenes in the 3D printed structures without affecting the quality of the fillers, as witnessed by XRD, XPS and electronic microscopy measurements. After carbonization, the 3D-printed structures maintained their complex shape, despite, a shrinkage of about 75% was measured. This requires that careful design of CAD should be performed to obtain objects with the desired final shape. At last, electrical measurements were performed to measure the capability for electronic application. Even if the resistance was decreased by one scale magnitude, these 3D printed MXenes/composites still need an improvement of their electric properties. To this end, the feasibility of 3D printing with this material on DLP suggests intriguing advancements in this technology, even if still a lot needs to be improved, especially in terms of electrical conductivity. The potential to develop 3D architectures through this method gives the possibility to create complex devices and further advanced electronic applications, achieving also good resolution, always considering proper compensation for the shrinkage of the material.

Author statement

A.S. Investigation and Writing - Original Draft.
H.P. Investigation, Data Curation and Writing - Review & Editing.
J. G. J. Investigation and Writing - Review & Editing.
S.B. Investigation and Writing - Review & Editing.
J.A. Resources and Writing - Review & Editing.
T.O. Resources and Writing - Review & Editing.
I.R. Supervision, Writing - Original Draft.
M.C. Funding acquisition and Writing - Review & Editing.

Declaration of competing interest

The authors declare that they have no known competing financial interests or personal relationships that could have appeared to influence the work reported in this paper.

Data availability

Data will be made available on request.

Acknowledgements

The authors would like to acknowledge Dr. Adriano Sacco for his support in electrical measurements.

Appendix A. Supplementary data

Supplementary data to this article can be found online at https://doi.org/10.1016/j.compositesb.2023.110854.

References

[1] Abdolhosseinzadeh S, Jiang X, Zhang H, Qiu J, Zhang C. Perspectives on solution processing of two-dimensional MXenes. Mater Today 2021;48:214–40.
[2] Iqbal A, Shahzad F, Hantanasirisakul K, Kim M-K, Kwon J, Hong J, et al. Anomalous absorption of electromagnetic waves by 2D transition metal carbonitride Ti_3CNT_x(MXene). Science 2020;369(6502):446–50.
[3] Anasori B, Gogotsi Y. 2D metal carbides and nitrides(MXenes). Cham: Springer; 2019.
[4] Lin Z, Barbara D, Taberna P-L, Van Aken KL, Anasori B, Gogotsi Y, et al. Capacitance of $Ti_3C_2T_x$ MXene in ionic liquid electrolyte. J Power Sources 2016; 326:575–9.
[5] Gogotsi Y, Anasori B. The rise of MXenes. ACS Nano 2019;13(8):8491–4.
[6] Chen W, Liu P, Liu Y, Liu Z. Recent advances in Two-dimensional $Ti_3C_2T_x$ MXene for flame retardant polymer materials. Chem Eng J 2022;446:137239.
[7] Shanto MAH, Chowdhury MI, Antu AB, Niloy NR, Alam N, Ullah MA, et al. MXene based Heterostructures for electrode materials of Batteries: a Review. IOP Conf Ser Mater Sci Eng 2022;1225(1):012018.
[8] Wan H, Liu N, Tang J, Wen Q, Xiao X. Substrate-independent $Ti_3C_2T_x$ MXene waterborne paint for terahertz absorption and shielding. ACS Nano 2021;15(8): 13646–52.
[9] Tao N, Zhang D, Li X, Lou D, Sun X, Wei C, et al. Near-infrared light-responsive hydrogels via peroxide-decorated MXene-initiated polymerization. Chem Sci 2019; 10(46):10765–71.
[10] Chia HL, Mayorga-Martinez CC, Antonatos N, Sofer Z, Gonzalez-Julian JJ, Webster RD, et al. MXene titanium carbide-based biosensor: strong dependence of exfoliation method on performance. Anal Chem 2020;92(3):2452–9.
[11] Liu H-J, Dong B. Recent advances and prospects of MXene-based materials for electrocatalysis and energy storage. Mater Today Phys 2021;20:100469.
[12] Barsoum MW. The $M_{N+1}AX_N$ phases: a new class of solids: thermodynamically stable nanolaminates. Prog Solid State Chem 2000;28(1):201–81.
[13] Carey M, Barsoum MW. MXene polymer nanocomposites: a review. Mater Today Adv 2021;9:100120.
[14] Li Y, Shao H, Lin Z, Lu J, Liu L, Duployer B, et al. A general Lewis acidic etching route for preparing MXenes with enhanced electrochemical performance in non-aqueous electrolyte. Nat Mater 2020;19(8):894–9.
[15] Chaudhary V, Ashraf N, Khalid M, Walvekar R, Yang Y, Kaushik A, et al. Emergence of MXene–polymer hybrid nanocomposites as high-performance next-generation chemiresistors for efficient air quality monitoring. Adv Funct Mater 2022;32(33):2112913.
[16] Jasim SA, Hadi JM, Opulencia MJC, Karim YS, Mahdi AB, Kadhim MM, et al. MXene/metal and polymer nanocomposites: preparation, properties, and applications. J Alloys Compd 2022;917:165404.

[17] Luo W, Ma Y, Li T, Thabet HK, Hou C, Ibrahim MM, et al. Overview of MXene/conducting polymer composites for supercapacitors. J Energy Storage 2022;52:105008.
[18] Naik TP, Singh I, Sharma AK. Processing of polymer matrix composites using microwave energy: a review. Compos Part A Appl Sci Manuf 2022;156:106870.
[19] Qin L, Tao Q, Liu X, Fahlman M, Halim J, Persson POÅ, et al. Polymer-MXene composite films formed by MXene-facilitated electrochemical polymerization for flexible solid-state microsupercapacitors. Nano Energy 2019;60:734–42.
[20] Shamsabadi AA, Isfahani AP, Salestan SK, Rahimpour A, Ghalei B, Sivaniah E, et al. Pushing rubbery polymer membranes to Be economic for CO_2 separation: embedment with $Ti_3C_2T_x$ MXene nanosheets. ACS Appl Mater Interfaces 2020;12(3):3984–92.
[21] Cui Y, Zhu J, Tong H, Zou R. Advanced perspectives on MXene composite nanomaterials: types synthetic methods, thermal energy utilization and 3D-printed techniques. iScience 2023;26(1):105824.
[22] Gross BC, Erkal JL, Lockwood SY, Chen C, Spence DM. Evaluation of 3D printing and its potential impact on biotechnology and the chemical sciences. Anal Chem 2014;86(7):3240–53.
[23] Zhang CJ, McKeon L, Kremer MP, Park SH, Ronan O, Seral-Ascaso A, et al. Additive-free MXene inks and direct printing of micro-supercapacitors. Nat Commun 2019;10(1):1795.
[24] Zhang J, Wan L, Gao Y, Fang X, Lu T, Pan L, et al. Highly stretchable and self-healable MXene/polyvinyl alcohol hydrogel electrode for wearable capacitive electronic skin. Adv Electron Mater 2019;5(7):1900285.
[25] Fu J, Taher SE, Abu Al-Rub RK, Zhang T, Chan V, Liao K. Engineering 3D-architected gyroid MXene scaffolds for ultrasensitive micromechanical sensing. Adv Eng Mater 2022;24(7):2101388.
[26] Li T, Chen T, Shen X, Shi HH, Jabari E, Naguib HE. A binder jet 3D printed MXene composite for strain sensing and energy storage application. Nanoscale Adv 2022;4(3):916–25.
[27] Aakyiir M, Tanner B, Yap PL, Rastin H, Tung TT, Losic D, et al. 3D printing interface-modified PDMS/MXene nanocomposites for stretchable conductors. J Mater Sci Technol 2022;117:174–82.
[28] Goyanes A, Det-Amornrat U, Wang J, Basit AW, Gaisford S. 3D scanning and 3D printing as innovative technologies for fabricating personalized topical drug delivery systems. J Contr Release 2016;234:41–8.
[29] Gonzalez G, Roppolo I, Pirri CF, Chiappone A. Current and emerging trends in polymeric 3D printed microfluidic devices. Addit Manuf 2022;55:102867.
[30] Lantean S, Roppolo I, Sangermano M, Pirri C, Chiappone A. Development of new hybrid acrylic/epoxy DLP-3D printable materials. Inventions 2018;3(2):29.
[31] Salas A, Zanatta M, Sans V, Roppolo I. Chemistry in light-induced 3D printing. ChemTexts 2023;9(1):4.
[32] Lantean S, Barrera G, Pirri CF, Tiberto P, Sangermano M, Roppolo I, et al. 3D printing of magnetoresponsive polymeric materials with tunable mechanical and magnetic properties by digital light processing. Adv Mater Technol 2019;4(11):1900505.
[33] Lantean S, Roppolo I, Sangermano M, Hayoun M, Dammak H, Barrera G, et al. Magnetoresponsive devices with programmable behavior using a customized commercial stereolithographic 3D printer. Adv Mater Technol 2022;7(11):2200288.
[34] Huang B, Zhou Z, Wei L, Song Q, Yu W, Zhou Y, et al. $Ti_3C_2T_x$ MXene as a novel functional photo blocker for stereolithographic 3D printing of multifunctional gels via Continuous Liquid Interface Production. Compos B Eng 2021;225:109261.
[35] Greaves M, Mende M, Wang J, Yang W, Barg S. Investigating the rheology of 2D titanium carbide (MXene) dispersions for colloidal processing: progress and challenges. J Mater Res 2021;36(22):4578–600.
[36] Tetik H, Orangi J, Yang G, Zhao K, Mujib SB, Singh G, et al. 3D printed MXene aerogels with truly 3D macrostructure and highly engineered microstructure for enhanced electrical and electrochemical performance. Adv Mater 2022;34(2):e2104980.
[37] Gonzalez G, Baruffaldi D, Martinengo C, Angelini A, Chiappone A, Roppolo I, et al. Materials testing for the development of biocompatible devices through vat-polymerization 3D printing. Nanomaterials 2020;10(9):1788.
[38] Gonzalez G, Chiappone A, Roppolo I, Fantino E, Bertana V, Perrucci F, et al. Development of 3D printable formulations containing CNT with enhanced electrical properties. Polymer 2017;109:246–53.
[39] Sangermano M, Pegel S, Pötschke P, Voit B. Antistatic epoxy coatings with carbon nanotubes obtained by cationic photopolymerization. Macromol Rapid Commun 2008;29(5):396–400.
[40] Cortés A, Cosola A, Sangermano M, Campo M, González Prolongo S, Pirri CF, et al. DLP 4D-printing of remotely, modularly, and selectively controllable shape memory polymer nanocomposites embedding carbon nanotubes. Adv Funct Mater 2021;31(50):2106774.
[41] Chiappone A, Roppolo I, Naretto E, Fantino E, Calignano F, Sangermano M, et al. Study of graphene oxide-based 3D printable composites: effect of the in situ reduction. Compos B Eng 2017;124:9–15.
[42] Gastaldi M, Cardano F, Zanetti M, Viscardi G, Barolo C, Bordiga S, et al. Functional dyes in polymeric 3D printing: applications and perspectives. ACS Mater Lett 2020;3(1):1–17.
[43] Fantino E, Chiappone A, Roppolo I, Manfredi D, Bongiovanni R, Pirri CF, et al. 3D printing of conductive complex structures with in situ generation of silver nanoparticles. Adv Mater 2016;28(19):3712–7.
[44] Yang W, Yang J, Byun JJ, Moissinac FP, Xu J, Haigh SJ, et al. 3D printing of freestanding MXene architectures for current-collector-free supercapacitors. Adv Mater 2019;31(37):e1902725.
[45] Yang Q, Beers MH, Mehta V, Gao T, Parkinson D. Effect of thermal annealing on the electrical conductivity of copper-tin polymer composites. ACS Appl Mater Interfaces 2017;9(1):958–64.
[46] Deng H, Bilotti E, Zhang R, Loos J, Peijs T. Effect of thermal annealing on the electrical conductivity of high-strength bicomponent polymer tapes containing carbon nanofillers. Synth Met 2010;160(5–6):337–44.
[47] Han M, Yin X, Wu H, Hou Z, Song C, Li X, et al. Ti_3C_2 MXenes with modified surface for high-performance electromagnetic absorption and shielding in the X-band. ACS Appl Mater Interfaces 2016;8(32):21011–9.
[48] Li Z, Wang L, Sun D, Zhang Y, Liu B, Hu Q, et al. Synthesis and thermal stability of two-dimensional carbide MXene Ti_3C_2. Mater Sci Eng B 2015;191:33–40.
[49] Wei J, Liao M, Ma A, Chen Y, Duan Z, Hou X, et al. Enhanced thermal conductivity of polydimethylsiloxane composites with carbon fiber. Compos Commun 2020;17:141–6.
[50] Pan Y, Fu L, Zhou Q, Wen Z, Lin CT, Yu J, et al. Flammability, thermal stability and mechanical properties of polyvinyl alcohol nanocomposites reinforced with delaminated $Ti_3C_2T_x$ (MXene). Polym Compos 2019;41(1):210–8.
[51] Ji B, Fan S, Ma X, Hu K, Wang L, Luan C, et al. Electromagnetic shielding behavior of heat-treated Ti3C2TX MXene accompanied by structural and phase changes. Carbon 2020;165:150–62.
[52] Liu R, Li W. High-thermal-stability and high-thermal-conductivity $Ti_3C_2T_x$ MXene/poly(vinyl alcohol) (PVA) composites. ACS Omega 2018;3(3):2609–17.
[53] Halim J, Cook KM, Naguib M, Eklund P, Gogotsi Y, Rosen J, et al. X-ray photoelectron spectroscopy of select multi-layered transition metal carbides (MXenes). Appl Surf Sci 2016;362:406–17.
[54] Peng C, Yang X, Li Y, Yu H, Wang H, Peng F. Hybrids of two-dimensional Ti_3C_2 and TiO_2 exposing {001} facets toward enhanced photocatalytic activity. ACS Appl Mater Interfaces 2016;8(9):6051–60.
[55] Rakhi RB, Ahmed B, Hedhili MN, Anjum DH, Alshareef HN. Effect of postetch annealing gas composition on the structural and electrochemical properties of Ti_2CT_x MXene electrodes for supercapacitor applications. Chem Mater 2015;27(15):5314–23.